UC Office of the President
Recent Work

Title

Carbon Nanotube Porins in Amphiphilic Block Copolymers as Fully Synthetic Mimics of Biological Membranes

Permalink

Journal

ISSN

Authors

Sanborn, Jeremy R
Chen, Xi
Yao, Yun-Chiao
et al.

Publication Date

2018-12-01

DOI

Peer reviewed

Carbon Nanotube Porins in Amphiphilic Block Copolymers as Fully Synthetic Mimics of Biological Membranes

Jeremy R. Sanborn, Xi Chen, Yun-Chiao Yao, Joshua A. Hammons, Ramya H. Tunuguntla, Yuliang Zhang, Christina C. Newcomb, Jennifer A. Soltis, James J. De Yoreo, Anthony Van Buuren, Atul N. Parikh, and Aleksandr Noy*

Biological membranes provide a fascinating example of a separation system that is multifunctional, tunable, precise, and efficient. Biomimetic membranes, which mimic the architecture of cellular membranes, have the potential to deliver significant improvements in specificity and permeability. Here, a fully synthetic biomimetic membrane is reported that incorporates ultra-efficient 1.5 nm diameter carbon nanotube porin (CNTPs) channels in a block-copolymer matrix. It is demonstrated that CNTPs maintain high proton and water permeability in these membranes. CNTPs can also mimic the behavior of biological gap junctions by forming bridges between vesicular compartments that allow transport of small molecules.

Energy-efficient molecular separations are fundamental to a number of modern industrial, environmental, and biomedical processes including large-scale water treatment, water desalination, kidney dialysis, sterile filtration, and manufacturing of pharmaceuticals.[1] Although synthetic polymeric membranes have come to dominate this application landscape, ever increasing demands continue to fuel the search for energy-efficient membranes that can provide both high selectivity and high permeability in the critical ca. 1 nm pore size.

Dr. J. R. Sanborn, X. Chen, Dr. Y.-C. Yao, Dr. J. A. Hammons,
Dr. R. H. Tunuguntla, Dr. Y. Zhang, Dr. A. Van Buuren, Dr. A. Noy
Physical and Life Sciences Directorate
Lawrence Livermore National Laboratory
Livermore, CA 94550, USA
E-mail: noy1@llnl.gov
Dr. J. R. Sanborn, Dr. A. N. Parikh
University of California Davis
Davis, CA 95616, USA
X. Chen, Dr. Y.-C. Yao, Dr. A. Noy
School of Natural Sciences
University of California Merced
Merced, CA 95343, USA
Dr. C. C. Newcomb, Dr. J. A. Soltis, Dr. J. J. De Yoreo
Physical Sciences Division
Pacific Northwest National Laboratory
Richland, WA 99354, USA
Dr. J. J. De Yoreo
Department of Materials Science and Engineering and Department of Chemistry
University of Washington
Seattle, WA 98195, USA

To this end, biological membranes represent an attractive alternative. To achieve high levels of selectivity and permeability for separation and transport of nanometer-scale solutes, cellular membranes adopt a structural paradigm that is fundamentally different from conventional polymer membrane materials. Cellular membranes use a solute-impermeable, amphiphilic bilayer matrix that incorporates a variety of highly specific nanopore proteins (e.g., porins, gated ion-channels, connexins, etc.), which shuttle molecular or ionic solutes across the cellular or sub-cellular boundaries and enable highly selective material exchange between the cells and their surroundings.[2,3]

Taking inspiration from biology, researchers made several efforts to pursue robust and scalable synthetic membranes that either incorporate or inherently emulate functional biological transport units. Recent studies demonstrated successful lipid bilayer incorporation of a number of artificial nanopores based on dendritic dipeptide scaffold,[4] G-quaruplexes,[5] and self-assembled pillar arenes.[6] Other notable classes of artificial membrane nanopores include peptide-based nanopores, 3D membrane cages,[7] and large and complex DNA origami nanopores.[8] We have recently introduced another class of artificial membrane nanopores based on carbon nanotube scaffolds: carbon nanotube porins (CNTPs).[9] CNTPs are short segments of lipid-coated, single-wall carbon nanotubes produced by sonication-cutting[10] that can insert into lipid membranes and form defined ca. 1 nm diameter membrane pores with atomically smooth hydrophobic walls that support transport of protons and water.[11,12] In addition, larger 1.5 nm diameter CNTPs enable transport of ions, macromolecular polymers, or ssDNA. CNTPs are unique among biomimetic nanopores because carbon nanotubes are robust and highly chemically resistant, which make them amenable for use in a wider range of separation processes including those that requiring harsh environments. Unfortunately, the lipid bilayer matrix, into which the CNTPs are embedded, almost completely negates these advantages since it is fragile and disassembles in non-aqueous environments or upon exposure to air.

A robust and flexible membrane matrix is thus another critical component of an artificial membrane. Many amphiphilic block copolymers form bilayer motifs (i.e., polymersomes) in their dilute suspensions,[13,14] making them a leading alternative

to lipid-based liposomal membranes. Compared to liposomes, polymersomes are mechanically more robust, and offer a wider range of membrane elasticities and degrees of passive membrane permeability.[13] For instance, higher bending moduli of polymer vesicles, 40–460 $k_B T$ (compared to 10–30 $k_B T$ for lipid vesicles) make them less prone to bending deformations and their lower stretching moduli (80–100 versus 250–1000 mN m^{-1} for vesicles) render them more resistant to strain-induced fractures, allowing them to withstand volume expansion/compression under osmotic stresses.[15] Moreover, compared to lipid membranes, single component, homogeneous polymer membranes in their fluid state have lower water permeabilities (0.7–10 versus 15–150 μm s^{-1})[16] and reduced lateral fluidities (0.1–0.01 versus 1–4 μm^2 s^{-1}).[17,18] Furthermore, a thicker hydrophobic core in polymer membranes (8–10 versus 3–4 nm for lipid bilayers) should provide a better match and consequently higher degree of stabilization for the average CNTP length of 10–12 nm (we also note that, due to the nature of the sonication-cutting procedure used to synthesize CNTPs, they show a wide-size distribution,[9] and thus a portion of CNTPs incorporated into polymersome membrane is still expected to protrude beyond the membrane).

Here, we report integration of CNTP channels into poly(butadiene)-poly(ethylene oxide) (PBD$_{22}$-PEO$_{14}$) polymer membranes, mimicking the structure, architecture, and basic functionality of biological membranes in an all-synthetic architecture. Proton and water transport measurements show that carbon nanotube porins maintain their high permeability in the polymer membrane environment. In a significant expansion of the CNTP platform capabilities, we also demonstrate that CNTPs embedded in polymersomes can transport small-molecule reagents between vesicular compartments opening new opportunities for delivery molecular reagents to vesicular compartments to initiate confined chemical reactions and mimic the sophisticated transport-mediated behaviors of biological gap junctions.

Materials. We used 1.5 nm diameter P2 CNTs (Carbon Solutions Inc.) to produce CNTPs. P2 CNTs contain a higher concentration of defects than the raw CNT stock that we used in previous studies[10,11] (as indicated by an increased *D*-band signal in the Raman spectra, see Figure S1, Supporting Information) and we found that these defects resulted in more efficient cutting and an increased yield of CNTPs. 1,2-dioleoyl-sn-glycero-3-phosphocholine (DOPC) and Rhodamine B 1,2-dioleoyl-sn-glycero-3-phosphoethanolamine (Rhodamine B DOPE) were obtained from Avanti Polar Lipids. PBD-PEO 1800 polymer (P10191) was obtained from Polymer Source Inc. Horseradish peroxidase (HRP, P6782), 8-Hydroxypyrene-1,3,6-trisulfonic acid trisodium salt (HPTS, H1529), luminol sodium salt (A4685), calcium chloride, hydrogen peroxide (216763), phosphate buffered saline (P4417), 4-(2-Hydroxyethyl)piperazine-1-ethanesulfonic acid (HEPES, RDD002), hydrochloric acid solution (H9892), sodium chloride (S7653), potassium chloride (P9333), and deuterium oxide (151882) were obtained from Sigma–Aldrich. Fluo-4 pentapotassium salt (F14200) was obtained from Thermo Fisher Scientific Inc. Pre-assembled extruders with 200 and 400 nm pore sizes were obtained from T&T Scientific Inc.

Vesicle preparation. PBD-PEO diblock-copolymer vesicle were made following previously described protocols with minor changes.[18] Briefly, 5 mg of PBD-PEO 1800 suspended in chloroform was deposited in a glass vial and dried under vacuum overnight to remove all traces of chloroform. The film was resuspended in buffer and heated to 70 °C for 30 min before stirring at 200 RPM for an additional 30 min to form multilamellar vesicles. To convert them into unilamellar vesicles, the solution was subjected to 10 freeze-thaw cycles and then heated to 70 °C prior to mechanical extrusion through 400 or 200 nm tract-etched membranes. To incorporate 1.5 nm diameter CNTPs into the polymersomes, we adapted the protocols developed for incorporating CNTPs into lipid vesicles.[19] We first dehydrated 0.5–1.5 mL of the appropriate CNTP solution for 30 min in a rotating desiccator heated to 50 °C. Dried film was hydrated with buffer (see the next section for details) and briefly bath-sonicated to ensure complete solubilization. This DOPC/CNT complex was then used to hydrate a dried PBD–PEO film to obtain a final polymer concentration of 5 mg·mL^{-1}. The solution was then heated to 70 °C and stirred for 1 h, then it underwent 10 cycles of the freeze-thaw treatment, followed by extrusion through a 400 nm polycarbonate filter. Finally, polymersomes were separated from unincorporated CNTPs with size-exclusion chromatography on an 8 cm long Sepharose CL-6B column. Purified vesicles were characterized with dynamic light scattering (Zetasizer Nano-ZS90, Malvern Instruments) with each measurement containing an average of at least 10 individual runs. DOPC and DOPC-CNTP liposomes were made as described previously.[19]

Measurements of proton permeability. Polymersomes and CNT-polymersome proton transport measurements followed the protocols previously described for measuring proton transport in DOPC-CNTP liposomes.[11] Briefly, polymersome-CNTP vesicles containing 10×10^{-3} M of the pH-sensitive HPTS dye in buffer (150×10^{-3} M NaCl, 30×10^{-3} M KCl, and 10×10^{-3} M HEPES, pH of 7.5). Separately, 2 mL of the same buffer adjusted to pH 6.9 was placed in a cuvette inside a fluorimeter (Fluoromax 4, Horiba) and equilibrated to room temperature for at least 5 min with constant stirring. 70 μL vesicle aliquots were added to the cuvette and the instrument recorded a time trace of the HTPS fluorescence (Em/Ex: 450/514 nm). Proton permeability was determined from these kinetics as described previously.[11]

Direct estimation of diblock copolymer/phospholipid concentration by a colorimetric assay. The amount of membrane amphiphile present in samples was measured using a colorimetric assay that was used previously for lipids[20] and diblock copolymers.[21] Briefly, 200 μL aliquots of samples were dried for 15 min in a rotating desiccator heated to 50 °C. The dried samples were then solubilized with 2 mL of chloroform, followed by the addition of 2 mL ammonium ferrothiocyanate. This solution was vortexed vigorously for 1 min and allowed to separate on the bench top. The bottom chloroform layer was carefully extracted with a Pasteur pipette and the absorbance was measured at 510 nm (488 nm) to quantify the polymer (lipid) mass. This analysis used a calibration curve prepared from samples of known lipid and polymer concentrations.

High-speed atomic force microscopy imaging of supported block-copolymer bilayers. All AFM imaging used a 1.5 mm diameter mica disk substrate glued on a glass rod of the HS-AFM sample stage. Mica surfaces were freshly cleaved prior to

sample deposition and a small aliquot of vesicles was placed on the sample with a pipette and incubated for 30 min at 70 °C. High-speed atomic force microscopy (HS-AFM) images of CNTPs were acquired in tapping mode at room temperature using an HS-AFM instrument (RIBM, Japan) equipped with ultrashort AFM cantilevers with custom-produced high-density carbon/diamond-like carbon tips (USC-F1.2-k0.15, NanoWorld, tip radius < 10 nm). The electron beam deposited carbon tips (radius < 10 nm) were also fabricated on the AFM cantilevers with the Zeiss Crossbeam 1540. For all imaging studies the HS-AFM fluid cell was filled with 120 μL of phosphate buffered saline. 128 × 128 pixel images were collected from a 200 × 200 nm area at a scan rate of 2 frames per second. The home-built Matlab2015 (MathWorks, Natick, MA) code was used to convert the raw HS-AFM images to ImageJ (National Institutes of Health, Bethesda, MD) stacks for further processing.

Cryogenic TEM measurements of CNTP-polymersomes. Specimens were prepared for cryogenic (cryo) TEM specimens by placing a 3 μL drop of sample onto a 200 mesh copper TEM grid coated with lacey carbon film (EMS). Grids were glow discharged prior to use (EasiGlow, Ted Pella). Grids were inserted into an FEI Vitrobot Mark IV (FEI, Hillsboro, OR) maintained at room temperature and 70% relative humidity and blotted with filter paper [blot time: 1 s, relaxation time: 1 s, blotting force: 1 (unitless parameter)]. The grid was then rapidly plunged into liquid ethane. All specimens were stored and handled under liquid nitrogen after vitrification. Specimens were imaged under low-dose conditions in an FEI Titan 80–300 Environmental TEM equipped with a field emission electron gun and operated at 300 kV. Specimens were transferred into the TEM while maintaining cryogenic conditions (−176 °C) by using a Gatan 626 cryo-TEM holder. Images were captured with an UltraScan 1000 2k x 2k charge capture device (CCD) camera (Gatan, Inc.) operated via Digital Micrograph (Gatan, Inc). Once recorded, images that were processed using ImageJ.

Small angle X-ray scattering. In order to determine whether the lipid and copolymer phase-separate in the CNTP-polymersomes, we collected small angle X-ray scattering (SAXS) from: pure polymersomes, pure liposomes, and CNTP-polymersomes in solution with concentration of 10, 10, and 12.9 mg mL^{-1}, respectively. Each suspension was pipetted into a capillary tube at beamline 4-2 at the Stanford Synchrotron Radiation Laboratory[22] and exposed to 12.5 keV X-rays. The scattered intensity from the vesicles was collected in the q-range: 0.02 Å^{-1} < q < 1.5 Å^{-1}, where q is defined as the magnitude of the scattering vector.[23] Sixty frames (1 s each) were collected using a beam size of 0.3 mm x 0.3 mm whilst oscillating the solution to thwart beam damage. There was little difference between the 60 different SAXS frames collected from each sample. Therefore, all frames were averaged to increase the signal-to-noise ratio of the data.

NIR absorption measurements. Near-IR (NIR) absorption was measured using a Cary 4000 UV–vis/NIR spectrometer (Agilent). Briefly, 100 μL of vesicles were aliquoted into glass vials and dehydrated in a rotary evaporator set to 55 °C until completely dry. Dried film was then resuspended with 200 μL of D$_2$O water and bath-sonicated until the sample solution appeared uniformly turbid. The absorbance was measured from 1800 to 200 nm at a scanning rate of 600 nm s^{-1} and a time interval of 0.1 s. The absorbance in the S$_{22}$ regime (900–1100 nm)[24] was selected and subtracted from measurements of polymer or lipid vesicles alone to determine the peak absorbance.

Water transport studies. Water permeabilities of CNTP-polymersomes or control polymersomes were determined using a stopped-flow instrument (SFM2000, BioLogic) and previously described protocols.[12] Briefly, vesicles were rapidly mixed in the stopped-flow instrument with a hypertonic buffer solution composed of 10 × 10^{-3} M HEPES (pH 7.5) and varying concentrations of HPTS (from 6.25 to 40 × 10^{-3} M) or poly(diallyldimethylammonium chloride (PDADMAC) (0.5%–4% (w/v)). The osmolarity of each buffer was verified with a freezing-point osmometer (Osmomat 3000, Gonotec) prior to the experiment. Light scattering data were acquired in the time interval between 50 and 500 μs, at 90° scattering angle, and a measured dead time of 0.7 ms. For each osmolyte concentration, we averaged at least three individual runs and the resulting kinetics were used to calculate the water permeability as described previously.[12] The reported value for water permeability was calculated from an average of three different vesicle preparations.

Raman spectroscopy of CNTPs. Raman spectra of dried CNTP aliquots were collected using a Nicolet Almega XR micro-Raman spectrometer at laser wavelengths of 633 nm and laser power was kept below 100 W cm^{-1} to avoid heating the samples.

Chemiluminescence assay. CNTP-polymersomes containing 50 U mL^{-1} of HRP (final encapsulation efficiency 1.3%) were formed in a 10 × 10^{-3} M HEPES buffer at pH 7.8. To prevent damage to the enzyme, we used four freeze-thaw cycles in the vesicle preparation instead of the 10 listed above. Once extruded and separated from unencapsulated protein with size exclusion chromatography, vesicle fractions were collected, combined, and used immediately. In a typical experiment, 100 μL of CNTP-polymersomes loaded with HRP were added to a cuvette containing 1.8 mL of 10 × 10^{-3} M HEPES, pH 7.8. After 5 min, 40 μL of 200 × 10^{-3} M luminol sodium salt and 66.7 μL of 30% hydrogen peroxide was added, in separate steps, to begin the reaction and luminol chemiluminescence signal at 432 nm was recorded in a Fluoromax-4 fluorometer with the excitation pathway blocked and under constant stirring.

Ca^{2+} vesicle docking assay. CNTP-polymersomes were formed in a 10 × 10^{-3} M HEPES buffer, pH 7.2, that also contained 100 × 10^{-6} M of calcium indicator dye Fluo-4 pentapotassium salt (final encapsulation efficiency 6.7%). DOPC liposomes that incorporated 60 × 10^{-3} M CaCl$_2$ were formed. After extrusion and size-exclusion chromatography purification both types vesicles were kept in a water bath at 23.6 °C. In a typical experiment, 100 μL of polymersome and liposome vesicles were pipetted into 2.8 mL of 10 × 10^{-3} M HEPES pH 7.2 in a cuvette in a fluorimeter (Fluoromax-4, Horiba), and Fluo-4 fluorescence kinetics (Ex:494/Em:514) was recorded under constant stirring and strict temperature control.

Vesicle fusion assay. CNTP-polymersomes, CNTP-liposomes, pure polymersomes, and pure liposomes were formed in 10 × 10^{-3} M HEPES buffer, pH 7.2. Pure polymersomes and liposomes contained 5% (w/w) rhodamine B DOPE such that rhodamine B fluorescence is self-quenched. In a typical experiment 100 μL of pure liposomes and 100 μL of CNTP-liposomes

**ADVANCED
SCIENCE NEWS**

www.advancedsciencenews.com

**ADVANCED
MATERIALS**

www.advmat.de

were added to a cuvette with 1.8 mL 10×10^{-3} M HEPES buffer (pH 7.2). Kinetics of membrane exchange was evaluated by observing dequenching of rhodamine B fluorescence (Ex./Em.: 543/565 nm) under constant stirring.

CNTP incorporation and characterization. We chose PBD_{22}-PEO_{14} (PBD-PEO 1800) diblock co-polymer (MW PBD:PEO of 1200:600) as a membrane matrix since it forms 10–12 nm thick polymer bilayers that provide an ideal match for CNTP length. Block-copolymer membranes were previously used to incorporate a variety of membrane proteins, such as aquaporin Z,[25] ATP synthase,[26] GPCRs,[27] and OmpF porins[28]; therefore, we expected that CNTPs would also incorporate into this membrane (**Figure 1**a). To insert CNTPs into the block-copolymer membranes, we modified previously developed procedures for inserting CNTPs into lipid matrices,[10,19] by adding elevated temperatures and constant stirring necessary for PBD-PEO 1800 to form vesicles.

Cryogenic TEM (cryoTEM) images of CNTP-polymersomes (Figure 1b) contain linear features within the polymersome membrane that likely correspond to CNTPs inserted in the membrane. These images also share broad similarity with the cryoTEM images that we reported previously for CNTPs inserted into lipid bilayers,[9] although the overall contrast between the nanotube and polymer matrix was significantly weaker (see Figure S2, Supporting Information). Since CNTPs were synthesized using lipid-assisted sonication cutting, a small amount of DOPC lipid was introduced into the polymersomes with the CNTPs. Although lipids and block copolymers readily form mixed membranes, we have performed SAXS studies to test whether this additional lipid component was

forming phase-separated lipid domains in the membrane that could sequester CNTPs.

SAXS profile of the CNTP-polymersome vesicles was clearly distinct from the profiles of the vesicles created with pure PB-PEO or DOPC (Figure 1c). Moreover, as the scattered intensity from non-interacting phases should be additive, we can expect the scattered intensity from vesicles containing phase-separated PB-PEO and DOPC bilayers should represent a linear combination of the scattering signals of each component in the q-range where the characteristic sizes of each of the bilayers scatter (this assumption would not be valid at lower range of q-values that would reflect the overall size of each phase). The SAXS profile obtained for CNTP polymersomes was distinctly different from those of pure polymer or lipid vesicles and cannot be obtained from a linear combination of those profiles (Figure 3c, dashed lines), arguing that in our samples PB-PEO and DOPC bilayer phases do not phase-separate into distinct polymer and lipid domains.

To characterize the morphology and dynamics of CNTPs in the polymersome membrane further, we fused the CNTP-containing polymersomes to a mica surface and imaged the resulting supported bilayer with HS-AFM. We previously showed that HS-AFM not only can visualize CNTPs in lipid bilayers, but also can capture real-time dynamics of CNTP diffusion in the bilayer plane.[29] HS-AFM movies of control polymersome layers showed flat layer morphology devoid of any sharp features. These movies and other AFM images indicated that polymersome bilayers had smooth morphology and were approximately 9 nm thick, which agrees with the ca. 7–11 nm thicknesses observed in the cryo-TEM images.

In contrast, HS-AFM images of CNTP-containing polymersomes (see Movie 1, Supporting Information) reveal multiple sharp features protruding by on average 1–2 nm above the membrane plane, which we attribute to the CNTPs (Figure 1d).

To quantify the CNTP content in CNTP-polymersome samples, we measured the NIR absorbance in the 1050 nm region, which corresponds to the S_{22} transitions in carbon nanotubes. This spectral region is convenient because water and block copolymers that we used have minimal signal in this range (See Figure S3, Supporting Information), simplifying background subtraction. CNTP-polymersome samples showed a clear adsorption peak in this region, which was absent in control samples; moreover, the magnitude of the S_{22} peak increased with the increased loading of CNTPs into the polymersomes, confirming that this signal originated from the CNTPs. To quantify the number
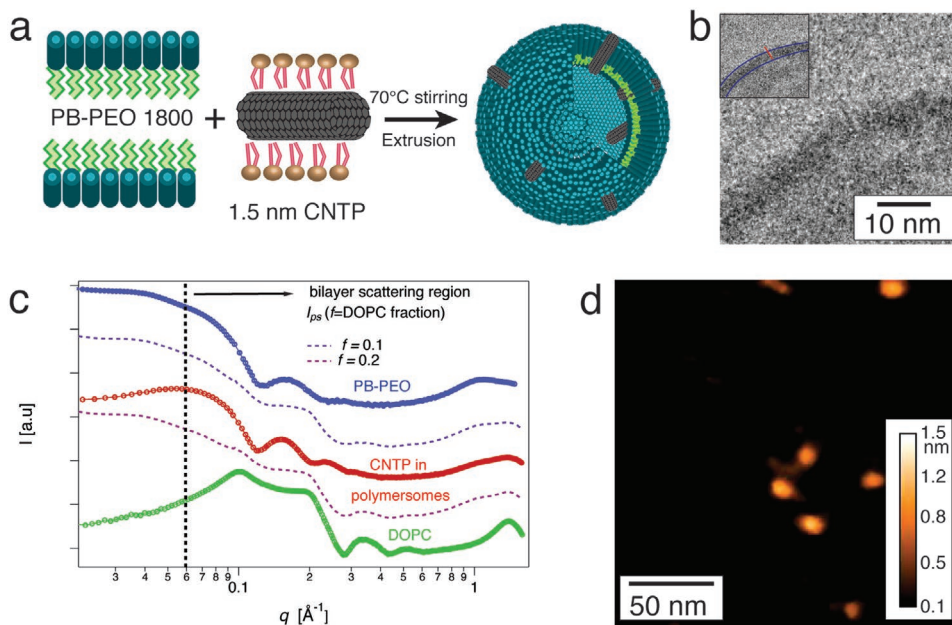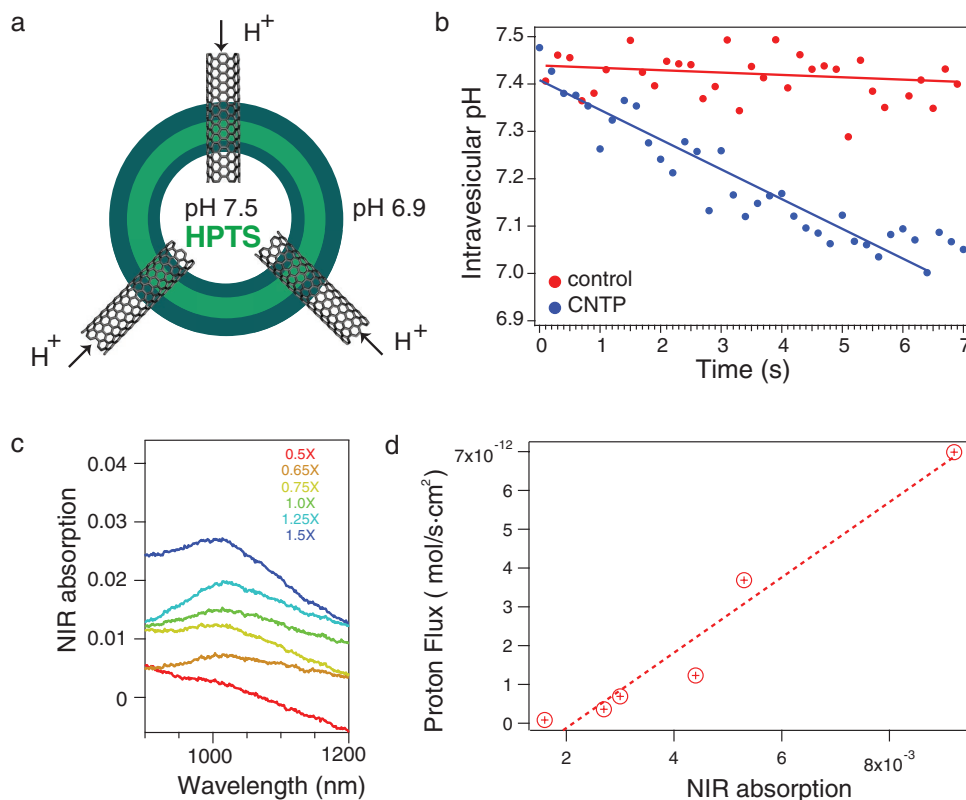

Figure 1. CNTPs in polymersome membranes. a) Schematic of the CNTP incorporation into PB-PEO 1800 polymersomes. b) Cryogenic TEM image of a polymersome wall with CNTPs. Inset highlights the location of the CNTP in the image. c) A log–log plot of the SAXS profiles for PB-PEO polymersomes (blue), DOPC liposomes (green), and CNTP-polymersomes (red). Dashed lines show predicted SAXS profiles for phase-separated PB-PEO and DOPC bilayers for lipid fraction of $f = 0.2$ (dark purple) and $f = 0.1$ (violet). d) A frame from a HS-AFM movie of the CNTP/polymersome membrane fused onto a mica surface. Image shows several CNTPs protruding above the polymersome membrane plane.

ADVANCED
SCIENCE NEWS
www.advancedsciencenews.com

ADVANCED
MATERIALS
www.advmat.de

of CNTPs in the polymer membrane we compared the magnitude of the S_{22} signal with the similar measurement performed on previously calibrated vesicle samples that contained CNTPs inserted into pure lipid bilayers. We then used this ratio of NIR signals (corrected for the difference in surface area of liposomes and polymersomes) to calculate the number of CNTPs present in polymersomes. Surprisingly, this comparison revealed that polymersome samples had 4 times more CNTPs compared to lipid samples formed under the same conditions. We attribute this effect to a better match between CNTPs length and the polymersome bilayer thickness. Furthermore, lower stretching moduli of polymer bilayers, compared to their lipid counterparts, may also contribute to favorable CNTP insertion. We also note that polymersome layers were previously shown to support nearly close-packed arrangement of artificial membrane channels,[6] suggesting that future work could potentially increase the CNTP loading.

Proton conductance measurements provide another way to characterize the number of CNTPs present in the polymersome membranes. When CNTPs-polymersomes were loaded with pH-sensitive HPTS dye in their lumen and exposed to a small pH gradient (**Figure 2**a), we observed rapid pH equilibration (Figure 2b) confirming that CNTPs in the polymer membrane serve as efficient proton transport conduits. Control polymersomes without CNTPs exhibited much slower pH equilibration kinetics; this is similar to our previous measurements of proton transport in CNTPs in lipid bilayers[11]

and indicates that the bulk of the proton flux in this system indeed flows through the CNTPs. Thus, it was not surprising that increased CNTP loading, quantified by an increase in S_{22} adsorption (Figure 2c), produced a corresponding increase in the proton flux through the CNTP polymersomes (Figure 2d). The unitary CNTP proton conductance $0.73 \times 10^{-7} \pm 0.41 \times 10^{-7}$ nS determined from these measurements (as the slope of the linear fit through the data on the Figure 2b) is within a factor of 3 of the unitary proton conductance value of $1.80 \times 10^{-7} \pm 0.69 \times 10^{-7}$ nS of CNTPs in lipid bilayers[11] This result could be expected, as the proton conductance rate primarily reflects the arrangement of the water hydrogen bonding pattern in the nanotube, but also can reflect the different nature of the surrounding membrane matrix.

Our previous stopped-flow measurements of water transport through CNTPs embedded in lipid membranes showed that they were highly efficient water conductors.[12] Here, we used similar protocols to investigate water transport through CNTPs in polymersomes (**Figure 3**). Like lipid vesicles, polymersome membranes are susceptible to complex osmotically induced shape changes, as has been previously reported for diblock polymersomes.[30] Thus, subtraction of the background water permeability of the polymersomes is not trivial in this case. Indeed, stopped-flow kinetics recorded after we subjected PBD-PEO 1800 polymersomes to an osmotic gradient (Figure 3B) revealed that instead of following a

Figure 2. Proton transport through CNTPs in polymersome membranes and optical properties of CNTPs. a) Schematic of the experiment. b) Initial time traces of the lumen pH values of polymersomes after pH of the outside solution decreased from 7.5 to 7.0. c) NIR absorption spectra in the S_{22} regime for increasing CNTP loading (as indicated in the legend) in CNTP-polymersomes. d) A plot of proton flux in CNTP-polymersomes as a function of S_{22} NIR absorption. Dashed line indicates a linear fit through the data.

**ADVANCED
SCIENCE NEWS**

www.advancedsciencenews.com

**ADVANCED
MATERIALS**

www.advmat.de
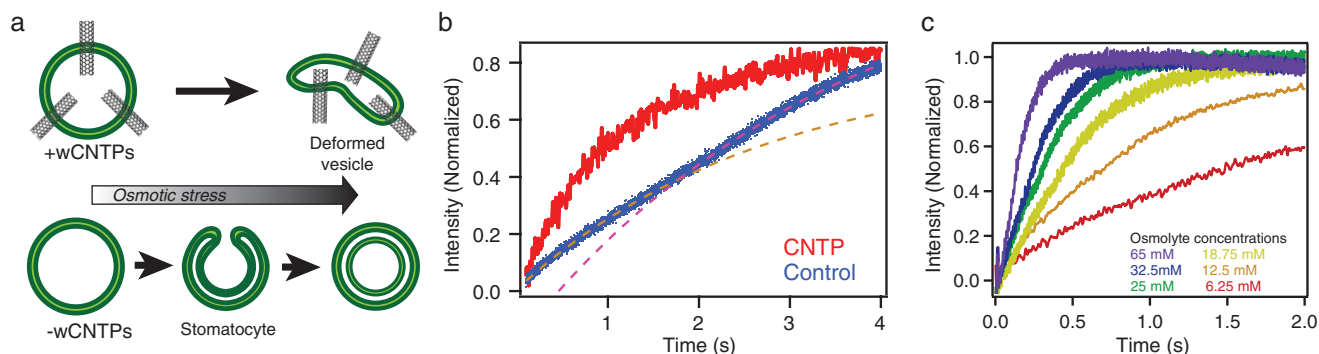
Figure 3. Water transport through CNTPs in polymersome membranes. a) Schematics showing different polymersome response to osmotic stress depending on the presence of CNTPs. b) Comparison of water transport kinetics from light scattering traces of hyperosmotic shocks of 0.5% PDADMAC acting on polymer vesicles with CNTPs and control vesicles without CNTPs, with two different fits (dashed lines) that approximate the general shape in the control trace. c) Light scattering traces taken from CNTP-polymersomes mixed with a series of HPTS concentrations.

single-exponential kinetics characteristic of gradual volume change, light scattering traces showed two distinct single-exponential kinetics regions, separated by a "shoulder" region (Figure 3b). Similar stopped-flow kinetic traces have also been previously recorded for DODAB vesicles.[31] As the osmotic stress increases, the location of the inflection point of the shoulder region shifts to earlier times (see Figure S4, Supporting Information) Following the models described in the literature, we speculated that osmotic response of polymersomes involved initial shrinkage followed by a structural transition to a deformed shape—most likely a variant of the "stomatocyte" shape—which then shrinks further as water transport across the membrane equalizes the osmotic imbalance (Figure 3a). Thus, we chose to use the first exponential region of the kinetic trace to extract the background polymersome water permeability. Our measured vesicle water permeability of ca. 30 µm s^{-1} is within the range of water permeability values reported for diblock copolymers, 2.5[32]–189.7 µm s^{-1},[33] even though a direct comparison with other studies may be complicated because the water permeability may be influenced by differences in aqueous buffer conditions and polymer chemistry.

When the polymersomes containing CNTPs were subjected to different levels of osmotic stresses, they showed much faster shrinkage kinetics and no clear shoulder was observed in the stopped-flow curves (Figure 3b,c) with only the lowest osmotic stress traces showing hints of the "stomatocyte" transition behavior. These results suggest that in the presence of a large number of CNTPs, which enable much faster water escape from the vesicle lumen, the "stomatocyte" shape transition is kinetically suppressed. We speculate that the transport behavior of CNTP-laden polymersomes is governed by a topological transformation, characterized by division of polymersome compartments consistent with continuous shrinkage that we observe. Such proposed mechanism is consistent with the previous observations and an elastic model proposed by Boroske and co-workers.[34] Specifically, the enhanced water flow can generate positive spontaneous curvature, thus providing conditions for the budding and fission of small, daughter vesicles.

Factors driving shape deformations of liposomes and polymersomes subject to hypertonic stresses are largely understood

in terms of minimal bending energy configurations of vesicles under conditions of reduced volume, $v = \dfrac{V}{[4\pi R_0^3/3]} < 1$ where R_0 corresponds to the radius of an equivalent sphere of area $S = [4\pi R_O^2]$.[35] These treatments implicitly assume that the vesicles adopt equilibrium shapes, which correspond to the smallest possible value of the membrane bending energy[36] and produce shape diagrams depicting shape morphologies (e.g., oblate, prolate, dumbbell, and stomatocytes) as a function of reduced volume.[37] Experimentally however, significant deviations from the predictions from these equilibrium shape diagrams, including budding, division, and tubulations, have also been observed most frequently associated with the generation of spontaneous membrane curvature through non-homogeneous distribution of membrane molecules.[38] Our present observations are consistent with (but do not independently establish) the idea that the high concentration of CNTPs in polymer membranes may be accompanied by generation of spontaneous curvature and lateral phase separation, which promote budding and division over stomatocyte shape transformations under hypertonic conditions.

The unitary permeability of CNTPs, measured in the stopped-flow data experiments was $7.7 \times 10^{-14} \pm 2.5 \times 10^{-14}$ cm^3 s^{-1} (see Figure S5, Supporting Information) These results agree with the water permeability that we previously reported for 1.5 nm diameter CNTPs embedded in lipid vesicles[12] (5.9×10^{-14} cm^3 s^{-1}), suggesting that the water transport mechanism in CNTPs is largely conserved between the two-membrane scaffolds. Notably, unlike the behavior that we observed in the experiments with lipid vesicles,[12] the water permeability was independent of the osmotic stress (see Figure S5, Supporting Information), which we attribute to the lower stretching moduli of the polymer membrane.

The experiments described in the previous sections show that CNTP channels in the walls of polymersomes facilitate mass exchange between the bulk solution and polymersome lumen. The small diameter of these channels should allow the CNTP-polymersomes to selectively encapsulate large molecules. This arrangement opens up a possibility to use CNTP polymersomes as nanoscale reactor compartments that contain and isolate some of the reaction
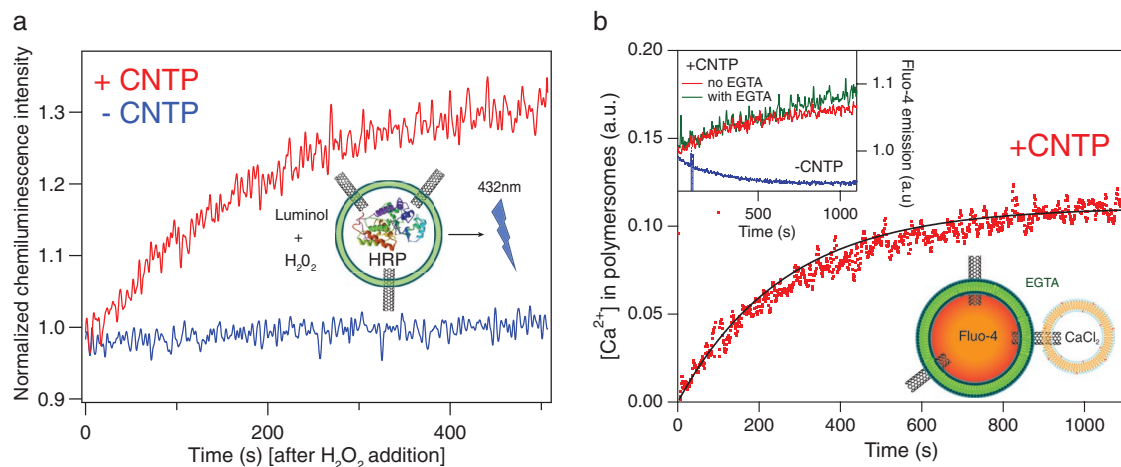
Figure 4. CNTPs as molecular exchange conduits. a) Chemiluminescence intensity recorded after adding luminol and hydrogen peroxide to the solution of polymersomes sequestering HRP enzyme in presence (red trace), and in absence (blue trace) of CNTPs in the polymersomes. Chemiluminescence signal was normalized to the signal recorded at the time $t = 0$. b) A graph showing an increase in the differential fluorescence intensity of a Ca^{2+} reporter dye Fluo-4 encapsulated inside polymersomes caused by diffusion of Ca^{2+} ions from liposomes to polymersomes through CNTP conduits (inset schematics). The solid line corresponds to the fit of the data to a first order kinetics: $F = F_{max} \cdot \left[1 - \exp\left(-\frac{t}{\tau} \right) \right]$, where $\tau = 260 \pm 4s$. Inset: Fluo-4 fluorescence kinetics recorded in absence (blue trace) and in presence (red trace) of CNTPs in the polymersome wall. The green trace was recorded at the same condition as the red trace, except a Ca^{2+} chelator EGTP was added to the extravesicular buffer solution.

components, whereas the other components can be delivered through the CNTPs. We first used this concept to demonstrate localized chemiluminescence production in CNTP-polymersomes. We placed an enzyme, HRP, into the lumen of polymersomes that contained CNTPs in their walls. At 44 kDa, HRP was too large to pass through the CNTPs and thus remained trapped inside the lumen. However the 1.5 nm CNTPs were still large enough to transport small organic molecules[39] such as luminol and hydrogen peroxide that react with HRP to produce chemiluminescence. Indeed, when we added luminol and H_2O_2 to this sample, we observed a strong increase in the chemiluminescence (**Figure 4**a). In contrast, when the polymersomes lacked the CNTP channels in the wall, addition of luminol and H_2O_2 did not increase chemiluminescence, showing that the encapsulated enzyme and the substrate remained spatially separated. These experiments demonstrated that 1.5 nm CNTPs facilitate the transport of small molecules and highlight the potential of CNTP-based nanoreactors to conduct cell-free reactions in the conditions that can simulate crowded intracellular environments.

Another interesting possibility is to use CNTPs as a nanoscale conduit for small-molecule exchange between two nanoscale compartments, mimicking the functionality of connexin channels, which form gap junctions that mediate direct cell–cell exchange of small molecules.[3] Our previous studies[9] indicated that CNTPs have a propensity to bridge two adjacent bilayers, forming a simplified mimic of a gap junction. Unfortunately, subsequent MD simulations also raised the possibility that this configuration could also facilitate membrane fusion after the nanotube bridges two lipid bilayers.[40] Thus, for a CNTP to act as a gap junction mimic this undesirable process needs to be suppressed.

We hypothesized that if a nanotube bridges two dissimilar membranes, e.g. a polymer and a lipid membrane, fusion cannot

occur. To test this hypothesis, we labeled a fraction of lipids with a self-quenching concentration of Rhodamine B-DOPE (see Methods, Figure S6, Supporting Information). Both the hemifusion and full fusion events[41] would lead to the dilution of the labeled lipid and dequenching of the dye. Indeed, we observed significant de-quenching (Figure S6, top trace, Supporting Information) when both populations of interacting vesicles (donor vesicles that contained CNTPs, and recipient vesicles that did not) were formed with lipid bilayers. In contrast, when we used CNTP-polymersomes as the donor vesicles, their interactions with the recipient liposomes did not show any dequenching (Figure S6, bottom trace, Supporting Information) indicating that, as expected, CNTPs did not facilitate fusion between vesicles made of dissimilar types of bilayers.

To demonstrate CNTP-mediated material exchange between two separate vesicular compartments, we encapsulated a large Ca^{2+} indicator dye Fluo-4, which should not escape through 1.5 nm diameter CNTPs, in the polymersomes and added them to the lipid vesicles that contained 60×10^{-3} M $CaCl_2$. As expected, we observed a clear increase in the Fluo-4 emission after mixing these two vesicle populations (Figure 4b), indicating that Ca^{2+} ions were able to diffuse into the polymersome interior through the CNTP connections formed between the two types of vesicles. We also observed a nearly identical increase in the Ca^{2+} reporter signal when we added a Ca^{2+} chelator EGTA to the extravesicular buffer solution (Figure 4b, inset, green trace), indicating that the majority of the fluorescence increase was indeed caused by Ca^{2+} ions traveling from one vesicular compartment to another directly through the CNTP. Significantly when CNTPs were absent from the polymersomes, (Figure 4b inset, blue trace), we did not observe Fluo-4 signal increase, confirming that CNTPs were required for Ca^{2+} diffusion between the two vesicular compartments. These experiments also point to an interesting possibility for designing versatile CNTP gap

**ADVANCED
SCIENCE NEWS**
www.advancedsciencenews.com

**ADVANCED
MATERIALS**
www.advmat.de

junction mimics that could tune the transport selectivity simply by using nanotube porins of different diameter.

Our results show that CNTPs can insert into the block-copolymer layers to form completely synthetic mimics of biological membranes. CNTPs form transmembrane pores in polymersomes similar to those formed in lipid bilayers, and we show that these pores also have similar transport properties, establishing CNTPs as a universal membrane channel mimic. In particular, CNTPs maintain high proton and water permeability similar to those we reported previously for lipid membranes. The ability to use CNTPs in non-lipid membrane matrices allowed us to construct more sophisticated transport systems with CNTPs not only facilitating transmembrane transport, but also enabling gap-junction-like communication between different population of vesicles. We believe that these findings enable a number of interesting possibilities for designing new biomaterials systems. CNTPs of different size and length can be used to control transport selectivity, to regulate the communication between compartments of synthetic proto-cells or between proto-cell and live cells, and to facilitate sophisticated cargo exchange in these systems.

Supporting Information

Supporting Information is available from the Wiley Online Library or from the author.

Conflict of Interest

The authors declare no conflict of interest.

[1] a) M. Mulder, *Basic Principles of Membrane Technology*, Springer, Dordrecht, The Netherlands **1996**; b) M. Shannon, P. Bohn, M. Elimelech, J. Georgiadis, B. Marinas, A. Mayes, *Nature* **2008**, *452*, 301; c) J. R. Werber, C. O. Osuji, M. Elimelech, *Nat. Rev. Mater.* **2016**, *1*, 16018.
[2] Y.-X. Shen, P. O. Saboe, I. T. Sines, M. Erbakan, M. Kumar, *J. Membr. Sci.* **2014**, *454*, 359.
[3] B. Alberts, D. Bray, J. Lewis, M. Raff, K. Roberts, J. D. Watson, *Molecular Biology of the Cell*, Garland Science, New York **2007**.
[4] V. Percec, A. E. Dulcey, V. S. K. Balagurusamy, Y. Miura, J. Smidrkal, M. Peterca, S. Nummelin, U. Edlund, S. D. Hudson, P. A. Heiney, H. Duan, S. N. Magonov, S. A. Vinogradov, *Nature* **2004**, *430*, 764.
[5] M. Barboiu, A. Gilles, *Acc. Chem. Res.* **2013**, *46*, 2814.
[6] Y.-x. Shen, W. Si, M. Erbakan, K. Decker, R. De Zorzi, P. O. Saboe, Y. J. Kang, S. Majd, P. J. Butler, T. Walz, A. Aksimentiev, J.-l. Hou, M. Kumar, *Proc. Natl. Acad. Sci. USA*, Dordrecht **2015**, *112*, 9810.
[7] B. P. Benke, P. Aich, Y. Kim, K. L. Kim, M. R. Rohman, S. Hong, I.-C. Hwang, E. H. Lee, J. H. Roh, K. Kim, *J. Am. Chem. Soc.* **2017**, *139*, 7432.
[8] a) M. Langecker, V. Arnaut, T. G. Martin, J. List, S. Renner, M. Mayer, H. Dietz, F. C. Simmel, *Science* **2012**, *338*, 932; b) A. Seifert, K. Göpfrich, J. R. Burns, N. Fertig, U. F. Keyser, S. Howorka, *ACS Nano* **2015**, *9*, 1117; c) S. Howorka, *Nat. Nanotechnol.* **2017**, *12*, 619.
[9] J. Geng, K. Kim, J. Zhang, R. Tunuguntla, L. Comolli, F. Allen, K. Cho, D. Munoz, Y. Wang, C. P. Grigoropoulos, C. M. Ajo-Franklin, A. Noy, *Nature* **2014**, *514*, 612.
[10] R. H. Tunuguntla, X. Chen, A. Belliveau, F. I. Allen, A. Noy, *J. Phys. Chem. A* **2017**, *121*, 3117.
[11] R. Tunuguntla, F. Allen, K. Kim, A. Bellivieau, A. Noy, *Nat. Nanotechnol.* **2016**, *11*, 639.
[12] R. Tunuguntla, R. Henley, Y.-C. Yao, T. A. Pham, M. Wanunu, A. Noy, *Science* **2017**, *357*, 792.
[13] D. E. Discher, A. Eisenberg, *Science* **2002**, *297*, 967.
[14] a) F. M. Menger, K. D. Gabrielson, *Angew. Chem. Int. Ed. Eng.* **1995**, *34*, 2091; b) K. T. Nam, S. A. Shelby, P. H. Choi, A. B. Marciel, R. Chen, L. Tan, T. K. Chu, R. A. Mesch, B. C. Lee, M. D. Connolly, C. Kisielowski, R. N. Zuckermann, *Nat. Mater.* **2010**, *9*, 454; c) S. I. Stupp, V. LeBonheur, K. Walker, L. S. Li, K. E. Huggins, M. Keser, A. Amstutz, *Science* **1997**, *276*, 384; d) L. F. Zhang, A. Eisenberg, *Science* **1995**, *268*, 1728.
[15] a) R. R. Tangorra, A. Operamolla, F. Milano, O. H. Omar, J. Henrard, R. Comparelli, F. Italiano, A. Agostiano, V. De Leo, R. Marotta, A. Falqui, G. M. Farinola, M. Trotta, *Photochem. Photobiol. Sci.* **2015**, *14*, 1844; b) R. J. R. W. Peters, M. Nijemeisland, J. C. M. van Hest, *Angew. Chem., Int. Ed.* **2015**, *54*, 9614; c) D. A. Christian, A. W. Tian, W. G. Ellenbroek, I. Levental, K. Rajagopal, P. A. Janmey, A. J. Liu, T. Baumgart, D. E. Discher, *Nat. Mater.* **2009**, *8*, 843.
[16] a) A. Carlsen, N. Glaser, J.-F. Le Meins, S. Lecommandoux, *Langmuir* **2011**, *27*, 4884; b) D. E. Discher, F. Ahmed, *Annu. Rev. Biomed. Eng.* **2006**, *8*, 323.
[17] a) B. M. Discher, Y.-Y. Won, D. S. Ege, J. C. Lee, F. S. Bates, D. E. Discher, D. A. Hammer, *Science* **1999**, *284*, 1143; b) M. Kang, M. Tuteja, A. Centrone, D. Topgaard, C. Leal, *Adv. Funct. Mater.* **2018**, *28*, 1704356.

[18] D. L. Gettel, J. Sanborn, M. A. Patel, H.-P. de Hoog, B. Liedberg, M. Nallani, A. N. Parikh, *J. Am. Chem. Soc.* **2014**, *136*, 10186.

[19] A. E. R. H. Tunuguntla, V. Frolov, A. Noy, *Nat. Protoc.* **2016**, *11*, 2029.

[20] J. C. M. Stewart, *Anal. Biochem.* **1980**, *104*, 10.

[21] O. Al-Hanbali, N. M. Onwuzo, K. J. Rutt, C. M. Dadswell, S. M. Moghimi, A. C. Hunter, *Anal. Biochem.* **2007**, *361*, 287.

[22] I. L. Smolsky, P. Liu, M. Niebuhr, K. Ito, T. M. Weiss, H. Tsuruta, *J. Appl. Crystallogr.* **2007**, *40*, s453.

[23] O. Glatter, O. Kratky, *Small Angle X-Ray Scattering*, Academic Press, New York, USA **1982**.

[24] A. L. Antaris, J.-W. T. Seo, A. A. Green, M. C. Hersam, *ACS Nano* **2010**, *4*, 4725.

[25] M. Kumar, M. Grzelakowski, J. Zilles, M. Clark, W. Meier, *Proc. Natl. Acad. Sci. USA* **2007**, *104*, 2071.

[26] H.-J. Choi, C. D. Montemagno, *Nano Lett.* **2005**, *5*, 2538.

[27] S. May, M. Andreasson-Ochsner, Z. Fu, Y. X. Low, D. Tan, H.-P. M. de Hoog, S. Ritz, M. Nallani, E.-K. Sinner, *Angew. Chem., Int. Ed.* **2013**, *52*, 749.

[28] W. Meier, C. Nardin, M. Winterhalter, *Angew. Chem.* **2000**, *112*, 4747.

[29] Y. Zhang, R. H. Tunuguntla, P.-O. Choi, A. Noy, *Philos. Trans. R. Soc. B: Biol. Sci.* **2017**, *372*, 20160226.

[30] R. Salva, J.-F. Le Meins, O. Sandre, A. Brûlet, M. Schmutz, P. Guenoun, S. Lecommandoux, *ACS Nano* **2013**, *7*, 9298.

[31] D. H. W. Hubert, M. Jung, P. M. Frederik, P. H. H. Bomans, J. Meuldijk, A. L. German, *Langmuir* **2000**, *16*, 8973.

[32] B. M. Discher, Y.-Y. Won, D. S. Ege, J. C.-M. Lee, F. S. Bates, D. E. Discher, D. A. Hammer, *Science* **1999**, *284*, 1143.

[33] M. Kumar, J. E. O. Habel, Y.-x. Shen, W. P. Meier, T. Walz, *J. Am. Chem. Soc.* **2012**, *134*, 18631.

[34] E. Boroske, M. Elwenspoek, W. Helfrich, *Biophys. J.* **1981**, *34*, 95.

[35] a) L. Miao, U. Seifert, M. Wortis, H. G. Dobereiner, *Phys. Rev. E* **1994**, *49*, 5389; b) B. L. S. Mui, H. G. Dobereiner, T. D. Madden, P. R. Cullis, *Biophys. J.* **1995**, *69*, 930.

[36] P. B. Canham, *J. Theor. Biol.* **1970**, *26*, 61.

[37] S. Svetina, B. Zeks, *Eur. Biophys. J.* **1989**, *17*, 101.

[38] a) H. G. Dobereiner, J. Kas, D. Noppl, I. Sprenger, E. Sackmann, *Biophys. J.* **1993**, *65*, 1396; b) M. Yanagisawa, M. Imai, T. Taniguchi, *Phys. Rev. Lett.* **2008**, *100*, 4.

[39] K. Kim, J. Geng, R. Tunuguntla, L. R. Comolli, C. P. Grigoropoulos, C. M. Ajo-Franklin, A. Noy, *Nano Lett.* **2014**, *14*, 7051.

[40] R. M. Bhaskara, S. M. Linker, M. Vögele, J. R. Köfinger, G. Hummer, *ACS Nano* **2017**, *11*, 1273.

[41] P. Wadhwani, J. Reichert, J. Bürck, A. S. Ulrich, *Eur. Biophys. J.* **2012**, *41*, 177.